

# RSC Advances



This is an *Accepted Manuscript*, which has been through the Royal Society of Chemistry peer review process and has been accepted for publication.

*Accepted Manuscripts* are published online shortly after acceptance, before technical editing, formatting and proof reading. Using this free service, authors can make their results available to the community, in citable form, before we publish the edited article. This *Accepted Manuscript* will be replaced by the edited, formatted and paginated article as soon as this is available.

You can find more information about *Accepted Manuscripts* in the [Information for Authors](#).

Please note that technical editing may introduce minor changes to the text and/or graphics, which may alter content. The journal's standard [Terms & Conditions](#) and the [Ethical guidelines](#) still apply. In no event shall the Royal Society of Chemistry be held responsible for any errors or omissions in this *Accepted Manuscript* or any consequences arising from the use of any information it contains.

**CONTROLLED SYNTHESIS AND CHARACTERIZATION OF ELECTRON RICH  
IRON (III) OXIDE DOPED NANOPOROUS ACTIVATED CARBON FOR  
CATALYTIC OXIDATION OF AQUEOUS ORTHO PHENYLENE DIAMINE**

**S.Karthikeyan, C. Judia Magthalin and A.B .Mandal G. Sekaran\***

*Environmental Technology Division, Council of Scientific & Industrial Research (CSIR) -  
Central Leather Research Institute (CLRI), Adyar, Chennai-600 020, Tamilnadu, India.*

\* Corresponding Author

Dr. G. Sekaran,

Chief Scientist & Cluster Chairman

Environmental Technology Division,

Central Leather Research Institute,

Adyar, Chennai – 600 020,

Tamil Nadu, India

Tel.: +91-44-24911386 (Extn: 7141)

Fax: +91-44-24452941

Email: [ganesansekaran@gmail.com](mailto:ganesansekaran@gmail.com)

## Abstract

This work deals with degradation of biorefractory aqueous ortho-phenylenediamine (OPD) by hydrogen peroxide and Iron (III) oxide doped Nanoporous activated carbon (Fe-NPAC). The Fe-NPAC was prepared by hydrothermal method. The catalyst was characterized using BET surface area and porosity analyzers, scanning electron microscope, transmission electron microscope, X-ray photoelectron spectroscopy (XPS), Fourier transform infrared spectroscopy (FT-IR), X-ray diffraction (XRD) and Thermo gravimetric analysis (TGA). The effect of pH, (1-10);, catalyst dosage, (Fe-NPAC, 0.1g, 0.2g, 0.3 g ); H<sub>2</sub>O<sub>2</sub> concentration, (1.76mmol, 3.52mmol, 5.29mmol, 7.05 mmol and 8.82 mmol) and effect of OPD concentration on the catalytic activity was evaluated. The catalytic oxidation of OPD by H<sub>2</sub>O<sub>2</sub>-Fe-NPAC<sub>400</sub> was confirmed using UV-Visible and Emission spectroscopy. The chemical oxygen demand (COD) was removed by 96% within 180 min in the presence of Fe-NPAC<sub>400</sub> which is about 20 folds higher than the control (without Fe-NPAC<sub>400</sub>). Moreover, Fe-NPAC<sub>400</sub> was demonstrated to have excellent stability and reusability characteristics.

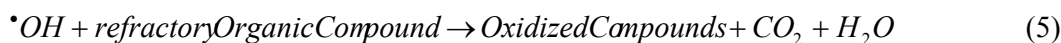
**Keywords:** *Fe-NPAC<sub>400</sub>, Heterogeneous Fenton oxidation, ortho-phenylenediamine, catalytic oxidation*

## Introduction

O-Phenylenediamine (OPD), an aromatic diamine belongs to nitrogen containing organic compound. OPD is processed into crop protection agents (45 %), dyestuffs (36 %), corrosion inhibitors (18 %), dyestuff catalysts (< 1 %), and photographic chemicals (< 1 %). Less than 1 % of the total amount is present in unknown compounds, analytical reagents, and therapeutic active ingredients<sup>1</sup>. They are widely used as raw materials or as intermediates in the manufacturing of industrial chemicals such as pesticides, drugs, dyestuffs, polymers, surfactants and cosmetics. OPD has been found to be hazardous in ingestion, inhalation, eye contact and they are carcinogenic, mutagenic<sup>2-4</sup>. Nitrogen containing groups, more often confer xenobiotic character to a synthetic compound<sup>5,6</sup>. Biological processes are the treatment systems that can usually remove readily biodegradable organics<sup>7</sup>. However, certain compounds such as OPD have been found to be persistent due to stabilised bonding and they are considered to be biorefractory organic compounds. Depending on their quantity and their eco toxicological behavior, the recalcitrant organics required additional treatment options for their removal<sup>8</sup>.

Existing treatment methods for the removal of aromatic amines from water include adsorption, extraction, microbial and chemical oxidation, electrochemical techniques, and irradiation. However, all of these methods suffer from serious shortcomings such as high cost, incompleteness of purification, formation of hazardous by-products, and low efficiency<sup>9</sup>. Thus, advanced oxidation processes (AOPs) have been developed to degrade bio refractory organic compounds in domestic water and industrial effluents<sup>10-12</sup>. The widely used AOP processes are UV photolytic technique<sup>13</sup>, Fenton process<sup>14-16</sup>, photo-Fenton process<sup>17,18</sup>, ozonation process<sup>19</sup>, sonolysis<sup>20-23</sup>, photocatalytic approach<sup>24-27</sup> and radiation induced degradation<sup>28-31</sup> especially for high content of organics, high colour intensity and non-

biodegradable contaminants<sup>32</sup>. Amongst several AOPs, Fenton oxidation has been widely used for its effectiveness to treat wastewater<sup>33</sup>. Fenton's reaction (combination of H<sub>2</sub>O<sub>2</sub> and Fe<sup>2+</sup>) has been demonstrated to rapidly degrade many organic compounds using insitu generated hydroxyl radicals (<sup>•</sup>OH). Due to the high oxidation potential(2.8V), fast reaction kinetics, and wide selectivity of the <sup>•</sup>OH toward most organics Fenton's reaction is capable of degrading organics into safe end products such as carbon dioxide, water, and organic acids such as formic acid, acetic, and oxalic acids<sup>34-36</sup>.



However, the homogeneous Fenton process has significant disadvantages such as narrow working pH range, iron containing sludge, and deactivation of iron ions. Therefore, the development of novel solid heterogeneous Fenton catalysts with improved stability has been strongly desired. To overcome these drawbacks, some efforts have been made to immobilise iron in suitable carrier matrices and termed heterogeneous Fenton-like catalysts<sup>37</sup>.

Nanoporous materials exhibit magnetic, optical, and reactive properties compared to corresponding bulk mesoporous materials, making them desirable for catalysis, adsorption, electronic sensing and medical applications<sup>38,39</sup>. Consequently, authors of this paper have been focusing on the application of Fenton system and nanoporous activated carbon for the treatment of wastewater discharged from different industries in recent years<sup>9,11,33</sup>. There has been constant research on the elimination of iron ions for the generation of hydroxyl radicals

to avoid metal ion pollution in the treated wastewater. The incorporation of iron (III) oxide into the structure of nanoporous activated carbon could ultimately minimize the metal leaching. However, reports on application of iron(III)oxide containing nanoporous activated carbon as a heterogeneous catalyst in AOP are very few or perhaps nil. Thus, an attempt has been made to use nanoporous activated carbon as an insoluble matrix for introducing the desired active sites for doping the iron (III) oxide and thereof for the degradation of OPD in aqueous solution.

### **Materials and methods**

Refractory organic compound, OPD, used in the present investigation was of reagent grade supplied by Sigma-Aldrich, Ferrous sulphate hepta-hydrate ( $\text{FeSO}_4 \cdot 7\text{H}_2\text{O}$ ), hydrogen peroxide (30 %w/v) and sulphuric acid (98 %) were purchased from Merck (Germany). The Fe-NPAC<sub>400</sub> prepared from rice husk in this laboratory was used in this study. The heterogeneous Fenton oxidation was carried out by dosing the OPD with  $\text{H}_2\text{O}_2$  (30% w/v) followed by the addition of Fe-NAC<sub>400</sub> (0.2 g/100ml).

### **Synthesis of Fe-NPAC Catalyst**

The nanoporous activated carbon prepared with phosphoric acid was soaked in hydrofluoric acid to remove silicon. The silicon removed NPAC was considered as a precursor for ferric oxide doping. The NPAC after the removal of silicon was oxidized using 5M nitric acid at its boiling point for 3 hours for incorporation of oxygen containing functional groups to allow surface complexation with metal ions<sup>46</sup>. The oxidized NPAC was doped with ferric iron by equilibrating with 0.05M Ferric nitrate solution for 2 hours followed by washing to remove the nitrate ion from the matrix. It was washed several times with deionised water to achieve neutral pH. The washed matrix was subjected to forced hydrolysis to form ferric hydroxide. It was calcined at different temperatures (300°C, 400°C

and 500°C) for 8 h to stabilise bonding of iron oxide in NPAC and it was labelled as Fe-NPAC.

### Characterization of Fe-NPAC

The BET surface area was measured by N<sub>2</sub> adsorption isotherm at 77 K using QUADRASORB SI automated surface area and pore size analyzer (Quantachrome Corporation, USA). Brunauer–Emmett–Teller (BET) and Horvath–Kawazoe (HK) methods were used to calculate the surface area and the pore size distribution of NPAC and Fe-NPAC. The morphology of the prepared Fe-NPAC was investigated using Scanning Electron Microscope (SEM, Quanta 200 FEG) combined with energy-dispersive X-ray spectroscopy (EDX) for mapping of elements, Transmission Electron Microscopy (TEM, TECNAI, PHILIPS, Netherlands) was used to evaluate the morphology and particle size of the NPAC and Fe-NPAC. X-ray diffraction (XRD) measurements of the supported Fe-NPAC heterogeneous catalyst were carried out on a Rich Siefert 3000 diffractometer under Cu- K $\alpha$ 1 radiation ( $\lambda=1.5406$  Å). X-ray photoelectron spectroscopy (XPS) was carried out in SPECS XPS system using 150W Al-K $\alpha$  radiation. High resolution spectra of C 1s, O 1s, N1s and Fe 2p core levels were obtained at pass energy of 25eV. The spectra were fitted with Gaussian-Lorentzian components to determine different oxidation states. The elemental composition (Carbon, Hydrogen, Nitrogen and sulphur) of the sample was determined using CHNS 1108 model Carlo – Erba analyzer. The Thermo Gravimetric Analysis (TGA) was carried out under nitrogen atmosphere from 30 to 800°C, with a temperature gradient of 10°C/min and scans were recorded using TGA Q50 (V20.6 Build 31). A Perkin-Elmer infra-red spectrophotometer was used for the investigation of the surface functional groups in NPAC and Fe-NPAC catalyst. UV–Vis spectroscopic measurements of the samples were performed on a Varian, CARY 100C double beam spectrophotometer using 1 cm quartz cuvette and scanned from  $\lambda_{200}$  to 800 nm. Total organic carbon content (TOC) was carried out using a Vario

TOC select V1.0.4 Elementar Analysen system GmbH (Liquid Model, Ser. No. 39101002) and Chemical oxygen demand were measured using a SPECTRA LAB Instruments.

## **Experimental section**

### **Heterogeneous Fenton oxidation process**

The batch experiments were carried out in a 1000-mL glass reactor vessel containing OPD solution of volume 100 mL (measured as 200ppm, 400ppm, 600ppm, 800ppm, and 1000ppm) that had been previously adjusted to different pH (1-10) using H<sub>2</sub>SO<sub>4</sub>/NaOH. The known concentration of OPD solution was dosed with Fe-NPAC<sub>400</sub> (0.2 g/100ml, 0.4g/100ml or 0.6 g/100ml) and H<sub>2</sub>O<sub>2</sub> (1.76mmol, 3.52mmol, 5.29mmol and 8.82) was added to initiate the oxidation reaction. The samples were collected at different time intervals and filtered. The filtered samples were used for further analysis. The used catalysts were pooled up, washed, dried and reused for oxidation of fresh OPD solution along with fresh H<sub>2</sub>O<sub>2</sub>

### **Analytical Methods**

Progress of OPD degradation by heterogeneous Fenton oxidation (Fe-NPAC<sub>400</sub>) was monitored through quantitative determination of chemical oxygen demand and Total organic carbon in accordance with standard methods for water and wastewater examination<sup>47</sup> (APHA 1998). The TOC was measured as per standard methods using Elementar Analysen system GmbH.

### **Iron leaching test**

After heterogeneous catalytic oxidation with hydrogen peroxide, the catalysts were removed by filtration and the total iron concentration in the liquid phase was determined using Atomic Absorption Spectrophotometer (Shimadzu AA 6650).

### **Stability and Reusability**

The recyclability of Fe-NPAC<sub>400</sub> catalyst was studied by using the catalyst in the successive batches of OPD degradation. The catalyst was first filtered through Whatman

No.1 filter paper, and dried in hot air oven at 110°C. It was resuspended in fresh solution of OPD and H<sub>2</sub>O<sub>2</sub> at the pre set pH, and the OPD degradation was continued as the second cycle. The same procedure was followed by subsequent cycles.

## Results and discussion

### Characterization of Fe-NPAC catalyst

#### Textural characteristics of Fe-NPAC

The porous frame work (surface area, pore diameter and pore volume) of the Fe-NPAC catalyst was established from surface area measured using the BET surface area analyser. Table 1 shows the surface area and pore diameter of the prepared Fe-NPAC and NPAC catalysts. Fig. 1 (A) and Fig.S1 (A) showed the adsorption isotherm and pore size distribution in the NPAC and Fe-NPAC<sub>400</sub> matrices. The surface area of nanoporous activated carbon was 153 m<sup>2</sup>g<sup>-1</sup>. The surface area of iron oxide doped NPAC prepared at 300<sup>0</sup>C; 400<sup>0</sup>C and 500<sup>0</sup>C were 105m<sup>2</sup>g<sup>-1</sup>, 38m<sup>2</sup>g<sup>-1</sup>, 136m<sup>2</sup>g<sup>-1</sup> respectively. The results are in good agreement with the fact that iron (III) oxide have been immobilised in the pores of NPAC leading to lowering of surface area. The lowering surface area of Fe-NPAC calcined at temperatures 300<sup>0</sup>C; 400<sup>0</sup>C and 500<sup>0</sup>C is mainly due to the packing of iron oxide in the pores. The minimum surface area in the calcined sample 400<sup>0</sup>C indicates the well-ordered and packed iron oxide. The iron hydroxide is there may decompose at 300<sup>0</sup>C and thereafter undergoes recrystallization leading to formation of fine grain sized oxide packed in the pores. The calcination at temperature 500<sup>0</sup>C, the surface area was increases may be due to grain growth of the immobilized iron oxide in the pores of NPAC. The calcined sample at 300<sup>0</sup>C, very low surface area than at 500<sup>0</sup>C, indicates the formation of iron oxide was not formed. Nano pore size distribution was calculated using the BJH method. The average pore diameter of the Fe (III) doped in carbon matrix approximately was equal to 5-6 nm. It is obvious that the Fe-

NPAC heterogeneous catalyst exhibited slightly wider pore size distribution than that of NPAC.

### **Phase structure and surface element composition of Fe-NPAC**

The chemical characteristics of the NPAC catalyst were carbon, 41.50%; hydrogen, 1.45%; nitrogen, 1.84%; sulphur, 0.11%, and iron, 0.5% for NPAC and that of Fe-NPAC were carbon, 38.20%; hydrogen, 1.51%; nitrogen, 1.56%; sulphur, 0.19%, and iron, 7.63% for Fe-NPAC<sub>400</sub> as shown in Table 2. The crystalline nature of synthesised Fe-NPAC is evident from the XRD pattern as presented in Fig. 1B. The 2theta value at 26.6° corresponds to reflection from graphite -like carbon and its broadening suggest that possible presence of an amorphous phase within the NPAC<sup>48</sup>. The XRD patterns show the nanostructure symmetry of replicated carbons as an indication of long range structural order. After heat treatment, the XRD diffraction pattern of the Fe-NPAC sample (Fig. 1B) shows the following d-values: 2.967, 2.527, 2.092, 1.714, 1.614, and 1.478 Å, they are related to (220), (313), (400), (422), (511), (440) Bragg diffraction planes of the iron (III) oxide (JCPDS file, PDF#89-5894). The XRD pattern of Fe-NPAC<sub>300</sub>, Fe-NPAC<sub>400</sub> and Fe-NPAC<sub>500</sub> catalysts showed the intensity of diffraction peak was varied. The relative intensity of the peaks was markedly increased with increase in calcination temperature from 300 to 500°C, being indicative of increase in the crystallinity of the catalyst. The XRD pattern of the composite after the heat treatment at 400°C and 500°C showed a high degree of crystallinity. The strong and sharp diffraction peaks indicate the good crystallinity in the prepared Fe-NPAC.

FT-IR spectra obtained with NPAC and Fe-NPAC samples are presented in Fig. 2A and Fig. 2B respectively. The broad band at 3338 cm<sup>-1</sup>(Fig. 2A) was associated with O–H stretching vibration mode of hydroxyl functional groups in NPAC. The stretching frequency at 2923 cm<sup>-1</sup> confirms the presence of CH<sub>2</sub> groups in NPAC. The bands at 950 cm<sup>-1</sup> and 1710

$\text{cm}^{-1}$  showed the presence of oxygen containing functional groups. The band at  $1621 \text{ cm}^{-1}$  was attributed to C=O vibrations in carbonyl groups and the band at  $1435 \text{ cm}^{-1}$  related to  $\text{COO}^-$  group. FTIR spectrum of iron-doped NPAC revealed that iron (III) oxide were distributed in the nanoporous activated carbon matrix containing surface functional groups such as  $-\text{OH}$ ,  $3338 \text{ cm}^{-1}$  and  $\text{COO}^-$ ,  $1435 \text{ cm}^{-1}$ . Fig.2A and Fig 2B show the FT-IR spectra of Fe-NPAC samples calcined at different temperatures. The peak at  $2915 \text{ cm}^{-1}$  was attributed to C-H stretching vibrations of Fe-NPAC at different molar concentration ranging from (0.02 to 0.05M) and at different temperatures ( $300^\circ\text{C}$ ,  $400^\circ\text{C}$  and  $500^\circ\text{C}$ ).

XPS measurements were conducted to investigate the oxidation states of iron in carbon matrix. Fig.3A shows the chemical components and the oxidation states of elements with high resolution. C1s, O 1s, N 1s and Fe 2p and Si 2p were highlighted in XPS spectrum. In core level XPS spectrum(Fig.3B), the C1s peaks at 285 eV, 290 eV, 288 eV, 287eV and 286 eV peaks are attributed to C1s of the C-C, carbonyl (C=O), amide (C-N) and carboxylic ( $\text{COO}^-$ ) functional groups present in NPAC<sup>48</sup>. Fig.3C shows the C1s spectra of the Fe-NPAC<sub>400</sub>, which could be resolved into four characteristic peaks. The binding energies at 286 eV, 287 eV, 288 eV and 289 eV were attributed to C=O,  $\text{COO}^-$  and amide (C-N) respectively. The XPS spectrum of the Fe-NPAC<sub>400</sub> exhibited a major peak at 533eV and 535eV in O1s core level spectrum, which are assigned to the iron (III) oxides and the residual oxygen containing functional groups present in the NPAC. Fig.3C shows the existence of iron oxide nano particle in carbon matrix with binding energies of about 711eV and 724 eV related to the Fe ( $2p_{3/2}$ ) and Fe ( $2p_{1/2}$ )<sup>49</sup>. Fig.3A displays the high- resolution XPS core level spectra of C1s characteristic peaks observed at 286 eV, 287 eV, 288eV and 290eV, respectively. The peaks confirmed the existence of C=O and  $\text{COO}^-$  groups. This indicates the bonding establishment of ferric ion with functional groups of NPAC through calcination. Fig.S1 (B) showed X-ray photoelectron spectra in NPAC and Fe-NPAC survey scan, Fig.S1(C) showed

XPS spectrum for the C1s region for the surface of the NPAC and after doped iron (III) nanoparticle on NPAC. Fig.S1 (D) showed photo luminescence (PL) spectrum of NPAC and Fe-NPAC.

SEM and EDX analyses were conducted to study the surface element distribution in the resultant Fe-NPAC<sub>400</sub>. The morphology of the catalysts NPAC and Fe-NPAC<sub>400</sub> are shown in Fig. 4 (A-D). The EDX profile corresponding to the SEM image confirmed the presence of iron (III) oxide nanoparticle in NPAC. The SEM images of NPAC and Fe-NPAC<sub>400</sub> showed that the iron (III) were uniformly distributed on the surface and in pores of carbon matrix, while the EDX image of the Fe-NPAC<sub>400</sub> confirmed the presence of iron (III) oxide in NPAC matrix. SEM analysis shown in Fig. 4A reveals irregular surface morphology of NPAC and the particle size varied in a wide range. By contrast, SEM morphology of the Fe-NPAC<sub>400</sub> catalyst (Fig. 4B) exhibited the presence of iron (III) oxide particles in NPAC matrix (see Figure S2 (B-F)). The iron (III) oxide formed a spherical shaped deposit onto both the exterior and interior walls of the NPAC, which assumed spherical shaped structure. The spherical shaped iron(III)oxide was further verified through high resolution transmission electron microscopy (HRTEM), where the oxide was differentiated from the NPAC substrate by its greater Z-contrast under the electron beam (see FigureS3, TEM image) the product is of numerous spherical shaped structures with uniform size distribution.

The structural arrangements in Fe-NPAC<sub>400</sub> were elucidated using high resolution transmission electron microscope (HRTEM) and selective area electron diffraction (SAED) images to investigate the microstructure of the catalyst. The amorphous catalyst has much structural distortion and therefore a much higher concentration of active sites for the catalytic reaction than its crystalline counterpart. Well-ordered arrays of iron oxide nanoparticle and pore channels are clearly observed. It can be seen that distribution of iron oxide nanoparticles are attached onto the wall surface of NPAC. The places with black dots in Fig.5 (A-D) could

be assigned to the deposition of iron oxide nanoparticle which were located in NPAC and occurred as small crystallites. A highly ordered array was observed, which was an indication for the preservation of the long-range arrangement of the iron nanoparticle in NPAC. The growth of these crystallites embedded into the nanostructured walls of the carbon, with spherical like crystallites formed after calcination. Such arrangements are obtained at the temperature of 400<sup>0</sup>C. The TEM image of Fe-NPAC<sub>400</sub> particles which are spherical in shape having an average diameter of ~ 4-6 nm as shown in Fig. 5A. The TEM image of the Fe-NPAC<sub>400</sub> catalyst showed that it was highly crystalline indicated by well-defined lattice fringes. The related SAED pattern (Fig.5B) showed that this Fe-NPAC<sub>400</sub> is polycrystalline nature. Fig.5C showed that the doped iron oxide nanoparticles were aggregated with an average diameter of ~4-6 nm and that each aggregate is also an assembly of many smaller iron oxide nanoparticles.

The TGA analysis was carried out from ambient temperature to 800<sup>0</sup>C with heating rate of 10<sup>0</sup> C/min under nitrogen atmosphere. The TGA profile provided information on thermal stability of NPAC and Fe-NPAC. Figure S4A shows the TGA spectrum of TGA for Fe-NPAC at different calcination temperatures 300<sup>0</sup>C, 400<sup>0</sup>C and 500<sup>0</sup>C. It shows the weight loss of the material at 101<sup>0</sup>C may be due to the removal of surface and bound water molecules present in the NPAC. The major mass change of 10.14%, 9.67% and 10.71% occurred at 344<sup>0</sup>C, 353<sup>0</sup>C and 388<sup>0</sup>C due to the decomposition of oxygen containing<sup>50</sup> functional groups present in the NPAC and Fe-NPAC. This indicates the strong binding of iron oxide nanoparticle deposit onto carbon matrix. Figure S4 B showed the TGA curve of NPAC and Fe-NPAC with different percentage of iron, it presents thermal degradation temperatures in two different ranges at 102 to 216<sup>0</sup>C. The weight loss platform was measured to be 6.87% at 101<sup>0</sup>C which can be attributed to the loss of coordinated water molecules. Thereafter, weight loss by 8.63% and 17.81% were observed at 216<sup>0</sup>C and 537<sup>0</sup>C

respectively, this could be due to the gasification of chemical deposit contributed by the pre-treatment process<sup>51</sup>. This was followed by weight loss of 27.06% up to 800°C and the residue left was 9.8 mg from the initial mass 13.41 mg.

### **Heterogeneous Fenton oxidation of OPD using Fe-NPAC<sub>400</sub> as catalyst**

#### **Effect of hydrogen peroxide on catalytic oxidation of OPD by Fe-NPAC<sub>400</sub>**

Hydrogen peroxide plays the role of an oxidizing agent in the heterogeneous Fenton reaction. Usually it has been observed that the percentage degradation of the pollutant increases with increase in the concentration of hydrogen peroxide<sup>52</sup>. It is the precursor in generating the hydroxyl radical<sup>53</sup>. To investigate the influence of the initial concentration of H<sub>2</sub>O<sub>2</sub> on the OPD degradation under the same catalytic dosage, the initial concentration of hydrogen peroxide was varied as 1.76mmol, 3.52mmol, 5.29mmol, 7.05 mmol and 8.82 mmol. The increase in H<sub>2</sub>O<sub>2</sub> concentration increased the rate of degradation of OPD. The increase in oxidant concentration from 1.764mmol to 8.82mmol led to an increase in the reaction rate<sup>55</sup>. Fig.6A showed that for heterogeneous Fenton oxidation by Fe-NPAC catalyst, the rapid mineralization and COD removal increased with decrease in loading of initial H<sub>2</sub>O<sub>2</sub> concentration during first 180 min.

#### **Effect of catalyst dosage Fe-NPAC<sub>400</sub> on OPD degradation**

Catalyst dose is the major parameter in oxidation reaction that catalytically decomposed the H<sub>2</sub>O<sub>2</sub> to generate ·OH free radicals. Catalyst concentration increased the oxidation efficiency because iron activates the hydrogen peroxide to generate hydroxyl radicals. An increase in the amount of Fe-NPAC dosage provided more iron (III) sites on the catalyst surface for accelerating the decomposition of H<sub>2</sub>O<sub>2</sub> which in turn increased the number of hydroxyl radical significantly<sup>56</sup>. The effect of dosage of Fe-NPAC<sub>400</sub> on the degradation of OPD was studied by varying the catalyst dosage from 0.2 to 1.0 g. Fig.6B reveals that the efficiency was enhanced at lower dosage of Fe-NPAC<sub>400</sub> and the same was

retarded at higher dosages. This is elucidated from the percentage of COD removal and mineralization of OPD. This is due to the scavenging effect of excess iron (III)oxide on the reactive HO<sup>•</sup><sup>57,58</sup>. Moreover, based on the ferrioxalate chemistry, there is an inhibition effect due to competition between the excess Fe (III) oxide and the pollutant molecules for the HO<sup>•</sup><sup>59</sup> at excess dosages of Fe-NPAC<sub>400</sub> over the optimal ratio with H<sub>2</sub>O<sub>2</sub>. The COD removal reached 96% within 180 min with low dosage of catalyst (0.2g/100ml), and for dosages 0.8 g and 1.0g the COD removal efficiencies were 88 % and 83 % respectively. The nanoporous carbon matrix support played a major role in the adsorption of the organic compounds and subsequent degradation resulted in a remarkable enhancement in heterogeneous Fenton oxidation process.

#### **Effect of OPD concentration**

The quantity of the OPD adsorbed on to the surface of the catalyst becomes very important because it determines the magnitude of degradation by heterogeneous Fenton oxidation. Concentration plays a very important role in reactions according to the collision theory of chemical reactions. Fig.6C shows the oxidative degradation of OPD at different concentrations (200 mg/L, 400 mg/L, 600 mg/L, 800 mg/L and 1000 mg/L) by maintaining other parameters constant. This implies that at higher initial concentration the degradation kinetics was highly concentration dependant. The removal of COD from OPD solution of concentration 200 ppm was almost complete within 180 min. This is due to stoichiometric ratio of number of molecules of OPD to number of available catalytic sites for degradation. However, further increase in the OPD concentration to 400 and 600 ppm the removal efficiency was decreased to 92% and 90% respectively due to decrease in effective collisions between the OPD dye molecules and °OH radicals. Fig.6D illustrates the kinetic model on effect of pH on OPD degradation by heterogeneous Fenton oxidation. It presents the comparison of the first and second order kinetics in fitting the experimental results. The

reaction rates and regression coefficient followed the pseudo first order kinetics, where  $C_t$  and  $C_0$  are the COD concentrations of OPD at time 't' and 0 minutes respectively and k is the rate constant<sup>61</sup>.

### Effect of pH

The pH of the solution plays a key role in the Fenton process, because it affects the solubility of Fe (II)/Fe (III), and ultimately controls the generation of  $\text{OH}^\circ$  radicals<sup>56</sup>. The effect of pH was carried out to determine the influence of pH from 1 to 10 on heterogeneous Fenton oxidation using Fe-NPAC<sub>400</sub>. In homogeneous Fenton oxidation phase, at pH 2.8 approximately half of the Ferrous ions supplied was present in the formation of  $\text{Fe}^{3+}$  ions and half of them was in the complex ion  $\text{Fe}(\text{OH})^{2+}$ . Lower values of pH results in depressing the concentration of  $\text{Fe}(\text{OH})^{2+}$ , while higher pH values results in precipitation of oxyhydroxides, both negatively affecting catalytic performance. Fig.7A to Fig 7C showed the COD and TOC values obtained at different pH values after 3 h of reaction time at room temperature. The degradation of OPD increased with increase in pH and the COD removal efficiency also followed the same pattern. The highest COD removal efficiency (96%) was recorded at pH 4 to 6, while it was 81% and 79% at pH 7 and pH 8 respectively. There was a sharp fall in degradation efficiency of OPD at pH higher than 6, and thus COD removal efficiency was decreased. The degradation efficiency of OPD by Fe-NPAC<sub>400</sub> was substantially high at low acidic condition as against high acidic condition generally reported in homogeneous oxidation. High acidity maintained using sulphuric acid in homogeneous Fenton oxidation increases the total dissolved solids content of wastewater. This presents an untreated condition for existing homogeneous Fenton oxidation for the oxidation of organics. Thus there has been constant exploration for the technology to perform at weakly acidic pH. This would substantially reduce total dissolved solids content of wastewater which is considered to be a challenge to environmental technologists.

The catalyst could be reused successive by for more than five runs without significant loss of activity. The mineralization of OPD could be monitored by TOC reduction during Heterogeneous Fenton oxidation for a period of 180 min. The results showed that Fe-NPAC<sub>400</sub> catalyst was able to hold its catalytic activity over a wide pH range.

### **Spectral evidences for degradation of OPD**

The UV-Visible spectrum of OPD (Fig.7D) has a characteristic peak at 420 nm. After heterogeneous Fenton oxidation, a new peak at 290 nm was appeared. This behaviour indicated the effective destruction of the nitrogen containing aromatic functional groups and breaking down of the aromatic rings of the OPD due to oxidation by °OH radicals. However, decolourisation of OPD was faster than that of its mineralization. This is because °OH radicals attack first the C-N bonds, which are of lowest energy, and then destructing the long conjugated  $\pi$  systems, the colour of OPD is due to non bonded electrons in amino group which may enter into resonance in benzene ring and thus stabilization of bonding was expected.

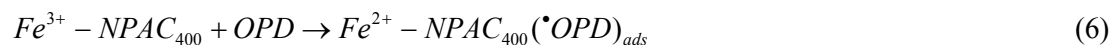
### **Stability of the Fe-NPAC<sub>400</sub>**

The recyclability of Fe-NPAC<sub>400</sub> heterogeneous Fenton catalyst was evaluated by batches degradation of reaction under optimum conditions. Since the catalytic stability and reusability are important factors in catalysis. It was found that the catalysts were able to reutilize for at least five cycles and retained its activity as efficient as fresh one. At the end of each process, the catalyst was removed and then washed gently with deionized water. The washed catalysts were dried in a hot air oven at 110 °C for 30 minutes to remove water molecules present on the surface of the catalyst. The reused catalyst showed the same degradation performance as in the case of the fresh one in subsequent repetitive cycles (Fig.8a). Three-dimensional fluorescence spectroscopy was used to record the emission profile of the OPD after heterogeneous Fenton oxidation by Fe-NPAC<sub>400</sub>. The emission

intensity of the treated water was decreased, which is an indication for degradation of the fluorophores present in the OPD. The shift in the fluorescence peak suggests the delocalization of  $\pi$ -electrons in the conjugate bond. OPD A red shift (longer wavelength is related to the amino group in the structures of the aromatic fluorophores) of OPD was transformed into blue shift after catalytic oxidation for 180 min, indicating the elimination of functional group such as amine. This may be attributed to the reduction in the degree of p-electron systems may be non bonded electrons in nitrogen of amino group, and the decrease in the number of aromatic rings and conjugated bonds in the open chain structure (Fig. 8b).

#### **Mechanistic view of mineralization of OPD in wastewater by Fe-NPAC<sub>400</sub>**

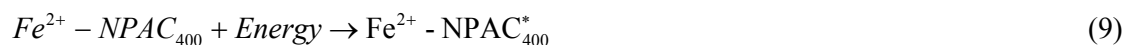
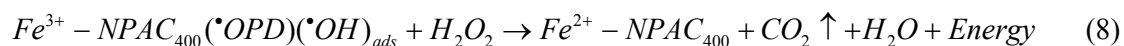
The iron (III) oxide nanoparticle in NPAC formed  $SP^3d^2$  overlapping with the oxygen and nitrogen functional groups of NPAC leaving behind unpaired electrons in 3d orbital of  $Fe^{3+}$  with strong paramagnetic behaviour (evidence from EPR signal confirmed with  $g \sim 4.01$  data not shown). The crystal field splitting energy must be high (as shown with strong emission at  $\lambda_{433}$  nm in Fluorescence spectroscopy) due to the presence of unpaired electrons. The unpaired electrons may serve to generate hydroxyl radicals from hydrogen peroxide, used as oxidant in heterogeneous Fenton oxidation of OPD in wastewater. The electron hole in the Fe-NPAC<sub>400</sub>, which has been confirmed as extrinsic semiconductor due to the presence of doped ferric ion, generates OPD radical as illustrated in (6)



The ferrous iron formed generates hydroxyl radical from hydrogen peroxide along with formation of ferric ion.



The ferric ion is reduced back to ferrous ion during the oxidation of OPD radical by hydroxyl radical



The algebraic sum of the chemical reaction such as (6-10) illustrate the generation of hydroxyl ions. This corroborate with the rise in pH of the OPD oxidized solution by 0.1 to 0.4 pH units.

The Fe-NPAC<sub>400</sub> as an integrated matrix to facilitate simultaneous adsorption and catalytic oxidation of OPD in wastewater. Pictorial representation of mechanistic view of Fe-NPAC<sub>400</sub> to produce hydroxyl radicals from H<sub>2</sub>O<sub>2</sub> (from external air supplied) for the oxidation of organics in OPD wastewater is shown in Fig. 9. The hydroxyl radicals are the oxidizing agents with high oxidation potential (2.8V) to facilitate the oxidation reaction at higher rate than in any other conventional technology used for the treatment of wastewater.

## Conclusion

In the present investigation the highly dynamic iron (III) oxide nanoparticle doped nanoporous activated carbon was prepared and characterized by different instrumentation techniques. Fe-NPAC<sub>400</sub> was used as heterogeneous Fenton catalyst to degrade and mineralize aqueous O-phenylene diamine. The Fe-NPAC<sub>400</sub> catalyst exhibited a high reactivity in heterogeneous Fenton oxidation to decolourise and remove COD by 96% within 180 min in the batch reactor at temperature, 37°C; catalyst dosage (Fe-NPAC<sub>400</sub>), 0.2 g/L; Initial pH, 7; The leaching of iron from Fe-NPAC<sub>400</sub> was only 0.3-0.4 mg in about 5 cycles and the recycle test confirmed the stability of catalyst for a long term application. The heterogeneous Fenton oxidation, using very low hydrogen peroxide concentration were used in the oxidation process and Fe-NPAC<sub>400</sub> (0.2 g/L), of OPD was by 96% at ambient conditions and at pH 6.0. The degradation of OPD was confirmed through instrumentation

techniques. This work would inspire further study regarding degradation of toxic organic compounds using this simple and stable heterogeneous Fenton system.

### Notes

The authors declare no competing financial interest.

### Acknowledgements

The authors are grateful to Council of Scientific and Industrial Research (CSIR) India, for financial assistance under STRAIT (CSC 0201) programme to carry out this work.

### S Supporting Information

Figure S1. (A) Pore size distribution of NPAC and Fe-NPAC<sub>400</sub>, (B) X-ray photoelectron spectra in NPAC and Fe-NPAC<sub>400</sub> survey scan, (C) XPS spectrum for the C1s region for the surface of the NPAC and after doped iron nanoparticle on NPAC (wine red colour), (D) Florescence emission spectrum of NPAC and Fe-NPAC<sub>400</sub>. The excitation at 220nm and it emits different wavelength (for NPAC), the excitation at 387nm, and emission-433nm (for Fe-NPAC<sub>400</sub>). Figure S2 (A) Typical SEM image of the NPAC with EDX, (B-E) SEM images of the Iron nanoparticle@ NPAC spheres at different magnifications, (E) Fe-NPAC<sub>400</sub> and the corresponding EDX, elemental composition (insets), Figure S3.TEM micrographs and the corresponding SAED patterns (insets) Fe-NPAC<sub>400</sub> at different magnitude. Figure S4(A) TGA curves of NPAC and Fe-NPAC@ different temperature, (B) TGA curves of NPAC and Fe-NPAC@ different percentage doped iron nanoparticle.

## References

- (1) S. Hirzel, Wissenschaftliche Verlagsgesellschaft, German Chemical Society Gesellschaft Deutscher Chemiker, GDCh-Advisory Committee on Existing Chemicals of Environmental Relevance (BUA), 1995.
- (2) T. Gichner, D. A. Stavreva, F. Van Breusegem, *Mutat. Res- Gen. Tox. Eng.*, 2001, 495, 117–125.
- (3) A. Nezamzadeh-Ejhieh, Z. Salimi, *Appl. Catal., A* 2010, 390, 110–118.
- (4) Yi-Hung Chen, Yi-You Liu, Rong-Hsien Lin, Fu-Shan Yen, *J. Hazard. Mater.*, 2009, 163, 973–981.
- (5) R. Campbell, *Microb. Ecol.*, 1977, New York: Blackwell. pp.148.
- (6) H. J. Knackmuss, *J Biotechnol.*, 1996, 51, 287-295.
- (7) L. C. Chiang, J. Chang, S. Tseng, *Water Sci. Technol.*, 1997, 36, 123-130.
- (8) H. Gulyas, *Water Sci. Technol.*, 1997, 36, 9-16.
- (9) A. Saupe, *Chemosphere* 1999, 39, 2325–2346.**
- (10) S. Karthikeyan, C. Anandan, J. Subramanian, G. Sekaran, *RSC Adv.*, 2013, 3, 15044–15057.
- (11) Chitra Kalyanaraman, K. Bala Kameswari, L. Vidya Devi, S. Porselvam, and J. Raghava Rao, *Ind. Eng. Chem. Res.*, 2012, 51, 16171–16181.
- (12) S. Karthikeyan, M. Ezhil Priya, R. Boopathy, M. Velan, A.B. Mandal and G. Sekaran, *Environ. Sci. Pollut. Res.*, 2012, 19, 1828-1840.

- (13) S. Gul , O. Ozcan-Yildirim, *Chem. Eng. J.*, 2009, 155, 684–690.
- (14) A. Masarwa, S. Rachmilovich-Calis, N. Meyerstein, D. Meyerstein, *Coordin. Chem. Rev.*, 2005, 249, 1937–1943.
- (15) E. Chamarro, A. Marco, S. Esplugas, *Water. Res.*, 2001, 35, 1047–1051.
- (16) C. Bouasla, M. E. H. Samar, F. Ismail, *Desalination*, 2010, 254, 35–41.
- (17) J. M. Monteagudo, A. Durán, I. S. Martín, M. Aguirre, *Appl. Catal. B-Environ.*, 2010, 95, 120–129.
- (18) A. K. Abdessalem, N. Bellakhal, N. Oturan, M. Dachraoui, M. A. Oturan, *Desalination*, 2010, 250, 450–455.
- (19) A. R. Tehrani-Bagha, N. M. Mahmoodi, F. M. Menger, *Desalination*, 2010, 260, 34–38.
- (20) S. Song, H. Ying, Z. He, J. Chen, *Chemosphere*, 2007, 66, 1782–1788.
- (21) H. Ghodbane, O. Hamdaoui, *Ultrason. Sonochem.*, 2009, 16, 455–461.
- (22) S. Merouani, O. Hamdaoui, F. Saoudi, M. Chiha, *Chem. Eng. J.*, 2010, 158, 550–557.
- (23) X. Wang, Z. Yao, J. Wang, W. Guo, G. Li, *Ultrason. Sonochem.*, 2008, 15, 43–48.
- (24) M. A. Rauf, M. A. Meetani, A. Khaleel, A. Ahmed, *Chem. Eng. J.*, 2010, 157, 373–378.
- (25) R. Xu, J. Li, J. Wang, X. Wang, B. Liu, B. Wang, X. Luan, X. Zhang, *Sol. Energ. Mat. Sol. C.*, 2010, 94, 1157–1165.
- (26) M. H. Habibi, N. Talebian, *Dyes Pigm.*, 2007, 73, 186–194.
- (27) S. B. Bukallah, M. A. Rauf, S. S. Ashraf, *Dyes Pigm.*, 2007, 72, 353–356.

- (28) A. Vahdat, S. H. Bahrami, M. Arami, A. Motahari, *Radiat. Phys. Chem.*, 2010, 79, 33–35.
- (29) K. A. Mohamed, A. A. Basfar, A. A. Al-Shahrani, *J. Hazard. Mater.*, 2009, 166, 810–814.
- (30) Y. P. Chen, S. Y. Liu, H. Q. Yu, H. Yin, Q. R. Li, *Chemosphere*, 2008, 72, 532–536.
- (31) K. Dajka, E. Takács, D. Solpan, L. Wojnárovits, O. Güven, *Radiat Phys. Chem.*, 2003, 67, 535–538.
- (32) G. Zhang, S. Wang, and J. F. Yang, *Phys. Chem. C.*, 2012, 116, 3623–3634.
- (33) S. Karthikeyan, G. Sekaran, V. K. Gupta, *Environ Sci. Pollut. Res.*, 2013, 20, 4790–4806.
- (34) M. Murugandham, M. Swaminathan, *Dyes Pigm.*, 2004, 63, 315–321.
- (35) J. H. Sun, S. P. Sun, M. H. Fan, H. Q. Guo, L. P. Qiao, R. Z. Sun, *J. Hazard Mater.*, 2007, 148, 172–177.
- (36) H. Zhang, D. Zhang, J. Zhou, *J. Hazard Mater.*, 2006, 135, 106–111.
- (37) J. I. Nieto-Juarez, K. Pierzchla, A. Sienkiewicz, T. Kohn, *Environ. Sci. Technol.*, 2010, 44, 3351–3356.
- (38) S. Enthaler, K. Junge, M. Beller, *Angew. Chem. Int. Ed. Engl.*, 2008, 47, 3317–21.
- (39) N. Tran, R. Pareta, E. Taylor, T.J. Webster, *Adv. Mater. Res.*, 2010, 89, 411–418.
- (40) D. L. Huber, *Small*, 2005, 1, 482–501.
- (41) J. I. Nieto-Juarez, K. Pierzchla, A. Sienkiewicz, T. Kohn, *Environ. Sci. Technol.*, 2010, 44, 3351–3356.

- (42) R. Chen, J. J. Pignatello, *Environ. Sci. Technol.*, 1997, 31, 2399–2406.
- (43) N. Kang, D. S. Lee, J. Yoon, *Chemosphere*, 2002, 47, 915–924.
- (44) S. Sabhi, J. Kiwi, *Water Res.*, 2001, 35, 1994–2002.
- (45) J. H. Ramirez, C. A. Costa, L. M. Madeira, G. Mata, M. A. Vicente, M. L. Rojas-Cervantes, A. J. Lopez-Peinado, R. M. Martin-Aranda, *Appl. Catal. B.*, 2007, 71, 44–51.
- (46) V. Fierroa, G. Muniza, G. Gonzalez-Sánchez, M. L. Ballinas, A. Celzarda, *J. Hazard. Mater.*, 2009, 168, 430–437.
- (47) APHA, American Public Health Association, Washington, 1998, DC
- (48) S. Karthikeyan and G. Sekaran, *Phys. Chem. Chem. Phys.*, DOI: 10.1039/c3cp54185a
- (49) C. Pereira, A. M. Pereira, P. Quaresma, P. B. Tavares, E. Pereira, J. P. Araujo and C. Freire, *Dalton Trans.*, 2010, 39, 2842–2854
- (50) J. Gong, K. Yao, J. Liu, Z. Jiang, X. Chen, X. Wen, E. Mijowska, N. Tiana and T. Tang, *J. Mater. Chem. A*, 2013, 1, 5247–5255
- (51) J. Zhu, X. Ouyang, M. Y. Lee, R. C. Davis, S. L. Scott, A. Fischer and A. Thomas, *RSC Advances*, 2012, 2, 121–124
- (52) S. H. Lin, C. M. Lin, H. G. Leu, *Water Res.*, 1999, 33, 1735–1741.
- (53) N. Masomboon, C. Ratanatamskul and Ming – Chunlu, *Environ. Sci. Technol.*, 2009, 43, 8629–8634.
- (54) P. Shukla, S. Wang, H. Sun, Hua-Ming Ang, M. Tade, *Chem. Eng. J.*, 2010, 164, 255–260.

- (55)M. Hartmann, S. Kullmann and H. Keller, *J. Mater. Chem.*, 2010, 20, 9002–9017.
- (56)H. Hassan, B. H. Hameed, *Int. J. Environ. Sci. Dev.*, 2011, 2, 218-222.
- (57)N. Daneshvar , M. A. Behnajady, Y. Z. Asghar, *J. Hazard. Mater.*, 2007, 139, 275-279.
- (58)B. Muthukumari, K. Selvam, I. Muthuvel, M. Swaminathan, *Chem. Eng. J.*, 2009, 153,9-15.
- (59)O. B. Ayodele, B. H. Hameed, *J.Ind.Eng. Chem.*, 2013, 19, 966–974.
- (60)J. Herney-Ramirez, A. Miguel. Vicente Luis M. Madeira, *Appl. Catal. B-Environ.*, 2010, 98, 10–26.
- (61)J. H. Sun, S. P. Sun, G. L. Wang, L. P. Qiao, *Dyes Pigm.*, 2007, 74, 647–652.

**Table 1.** Surface Area, and pore volume of NPAC and the Fe-NPAC

<b>Samples</b>	<b>Total surface area(m<sup>2</sup>/g)</b>	<b>S<sub>meso</sub> (m<sup>2</sup>/g)</b>	<b>S<sub>micro</sub> (m<sup>2</sup>/g)</b>	<b>V<sub>micro</sub> (cm<sup>3</sup>/g)</b>	<b>V<sub>meso</sub> (cm<sup>3</sup>/g)</b>
<b>NPAC</b>	153	119	33	0.0172	0.172
<b>Fe-NPAC<sub>300</sub></b>	105	57	48	0.020	0.071
<b>Fe-NPAC<sub>400</sub></b>	38	36	02	0.0021	0.069
<b>Fe-NPAC<sub>500</sub></b>	136	73	64	0.0279	0.098

**Table 2.** Elemental composition (CHNS analysis) of NPAC and Fe-NPAC

<b>Name</b>	<b>Weight (mg)</b>	<b>N (%)</b>	<b>C (%)</b>	<b>H (%)</b>	<b>S (%)</b>	<b>C/N ratio</b>	<b>C/H ratio</b>	<b>Fe (%)</b>
<b>NPAC</b>	4.20	1.84	41.50	1.45	0.11	22.51	28.63	0.5
<b>Fe-NPAC<sub>300</sub></b>	4.03	1.42	37.14	1.46	0.17	26.21	25.43	5.24
<b>Fe-NPAC<sub>400</sub></b>	3.92	1.56	38.20	1.51	0.19	24.70	25.27	7.63
<b>Fe-NPAC<sub>500</sub></b>	4.17	1.38	39.96	1.67	0.16	28.90	24.00	6.56

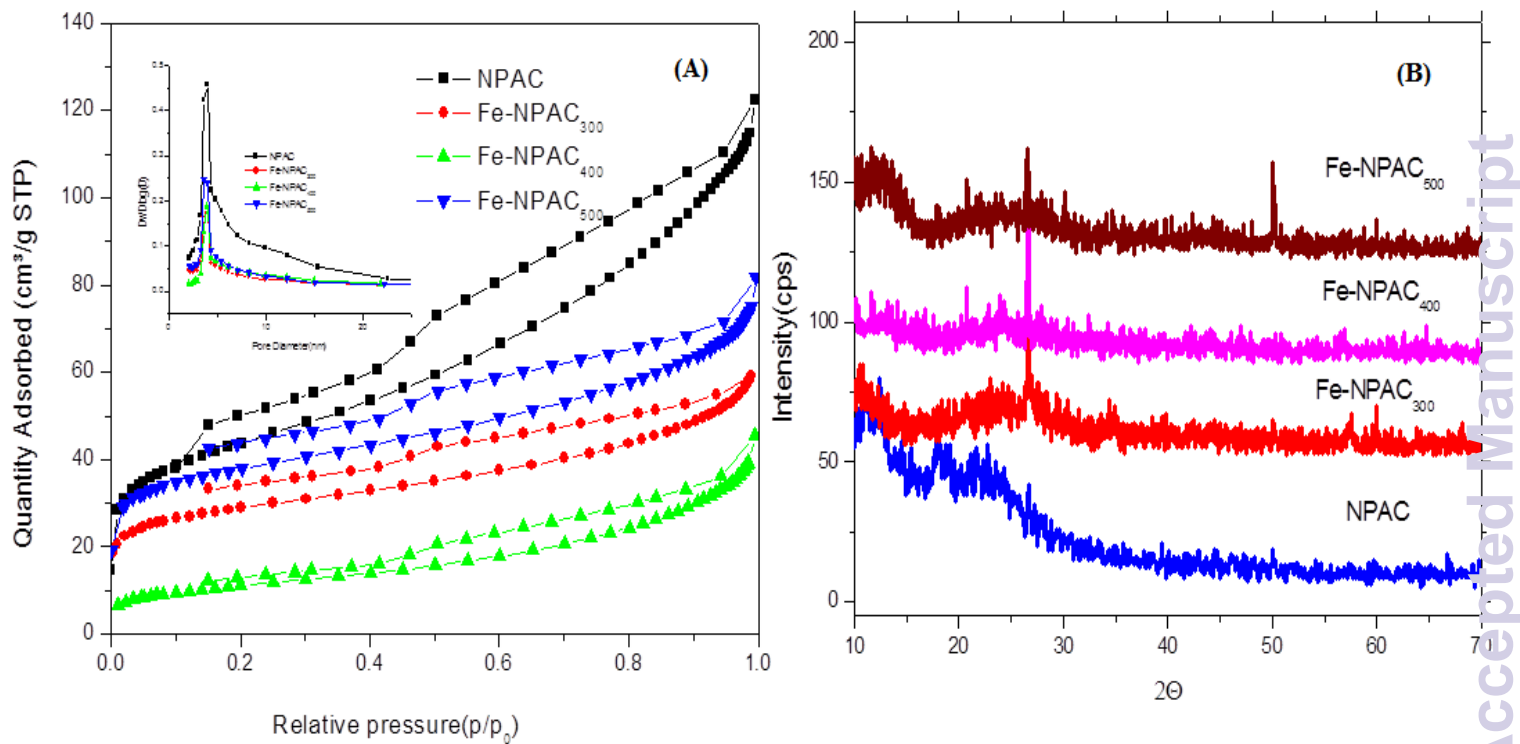


Fig. 1 (A) Adsorption isotherm and pore size distribution of the resulting NPAC and Fe-NPAC samples, (B) X-ray diffraction of patterns of NPAC and Fe-NPAC

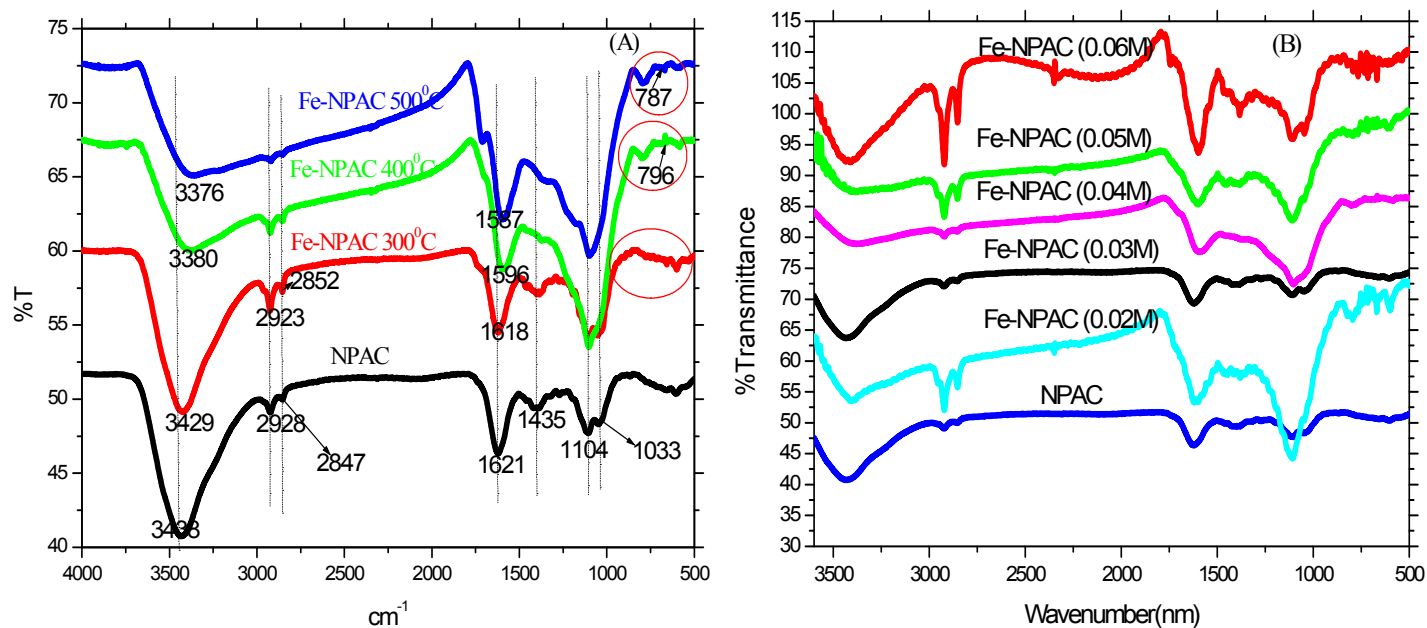


Fig.2(A) FTIR spectra of NPAC and doped iron nanoparticle on NPAC @different temperature, (B) FTIR spectra of NPAC and doped iron nanoparticle on NPAC @different temperature, the data was normalized with respect to the minimum transmittance.

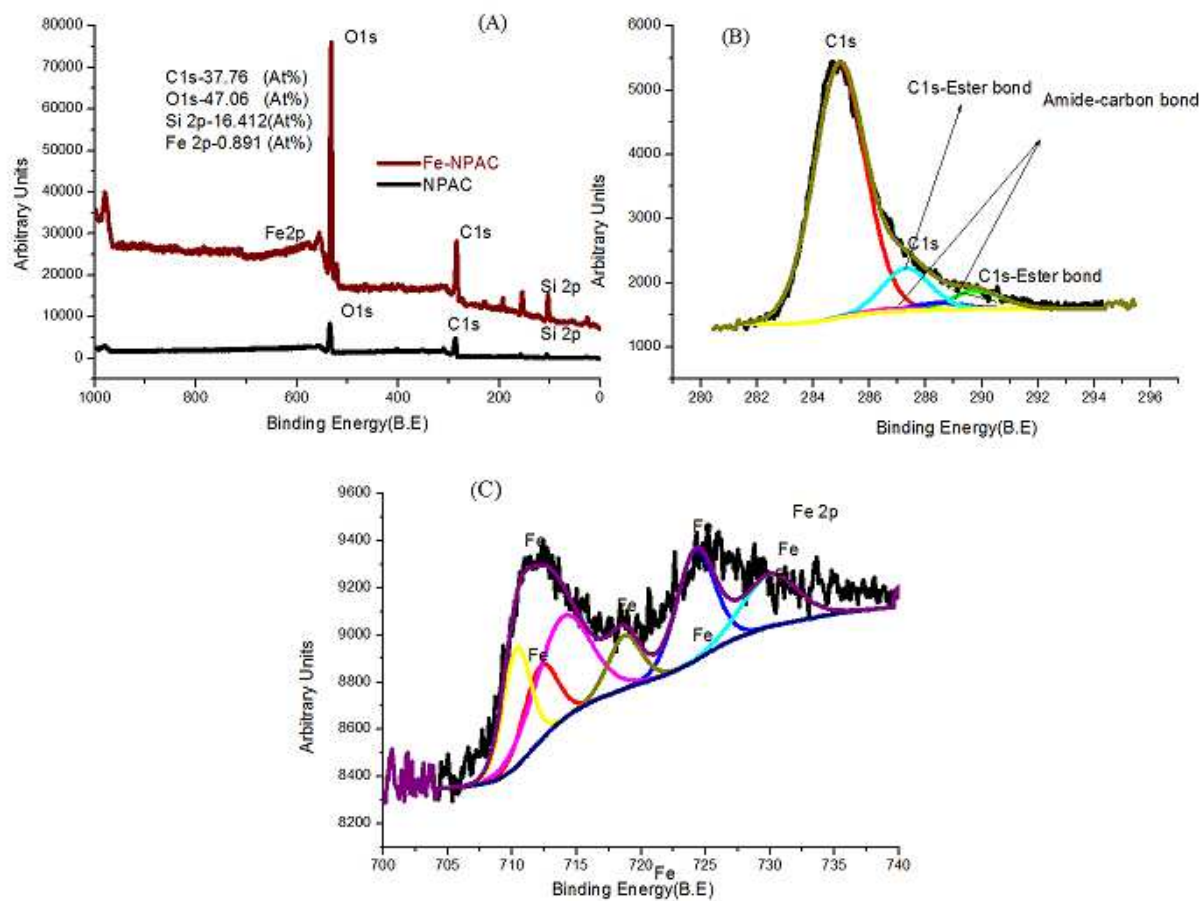


Fig.3 (A) X-ray photoelectron spectra in NPAC and Fe-NPAC survey scan, (B) XPS spectrum for the C 1s spectrum for the surface of the NPAC and after doped iron nanoparticle on NPAC, (C) XPS spectrum for Fe 2p binding

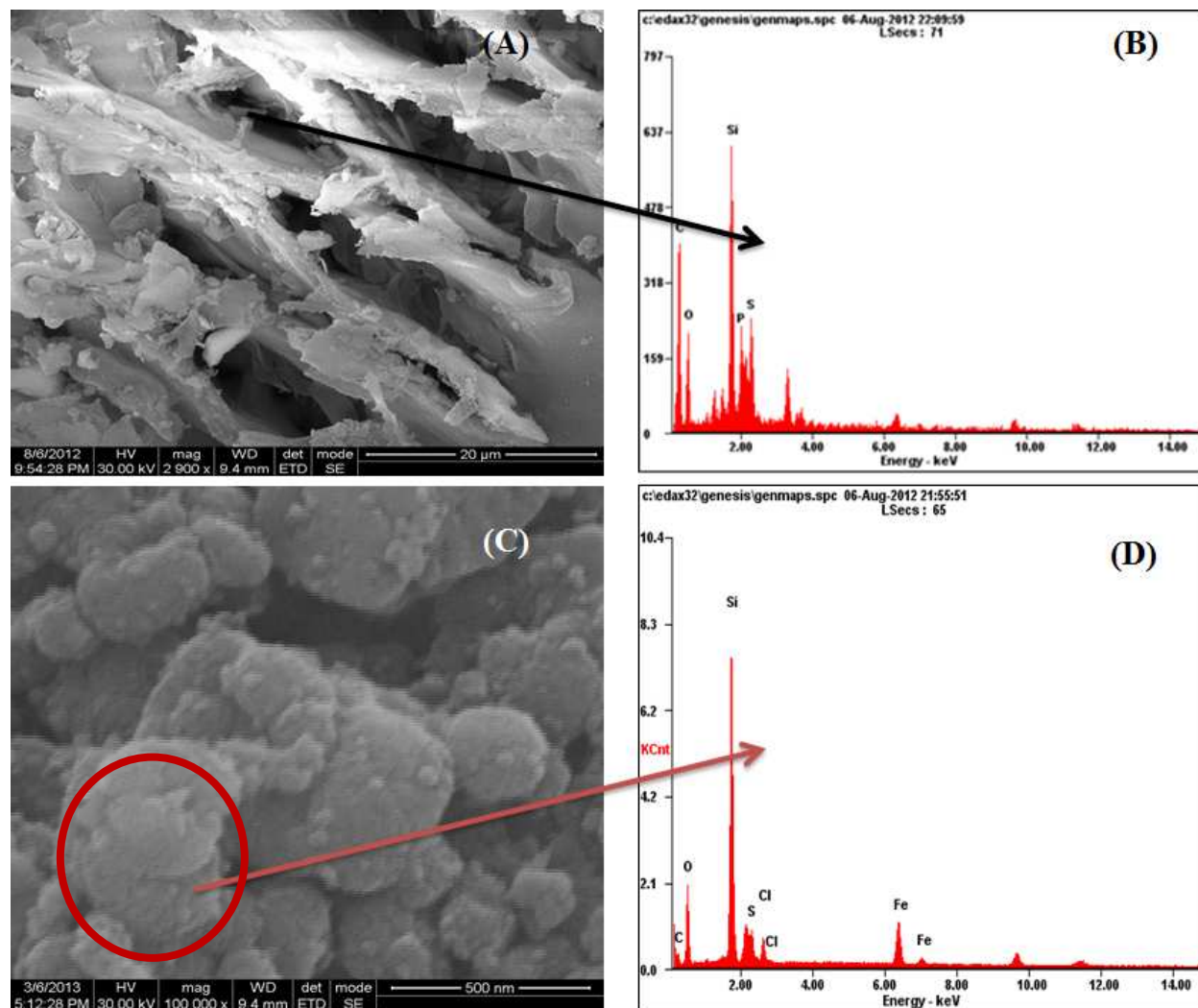


Fig. 4 (A) HRSEM image of thermal-treated NPAC, (B) thermal-treated NPAC with corresponding EDX spectrum, (C) HRSEM image of thermal-treated Fe-NPAC<sub>400</sub>, (D) Thermal-treated Fe-NPAC<sub>400</sub> with corresponding EDX spectrum.

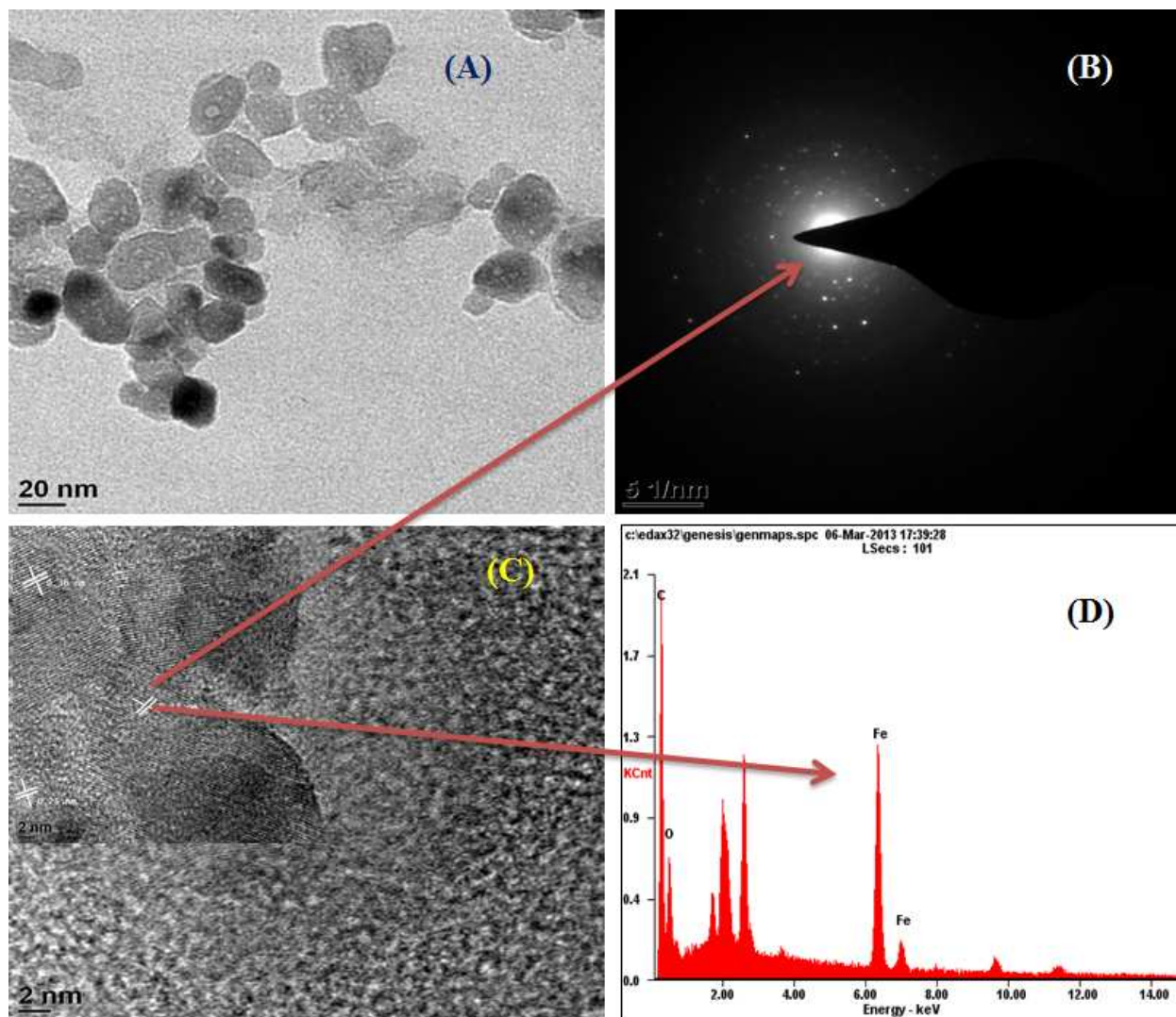


Fig. 5 (A) HRTEM image of thermal-treated NPAC, (B) thermal-treated NPAC with corresponding EDX spectrum, (C) HRTEM image of thermal-treated Fe-NPAC<sub>400</sub>, (D) Thermal-treated Fe-NPAC<sub>400</sub> with corresponding EDX spectrum.

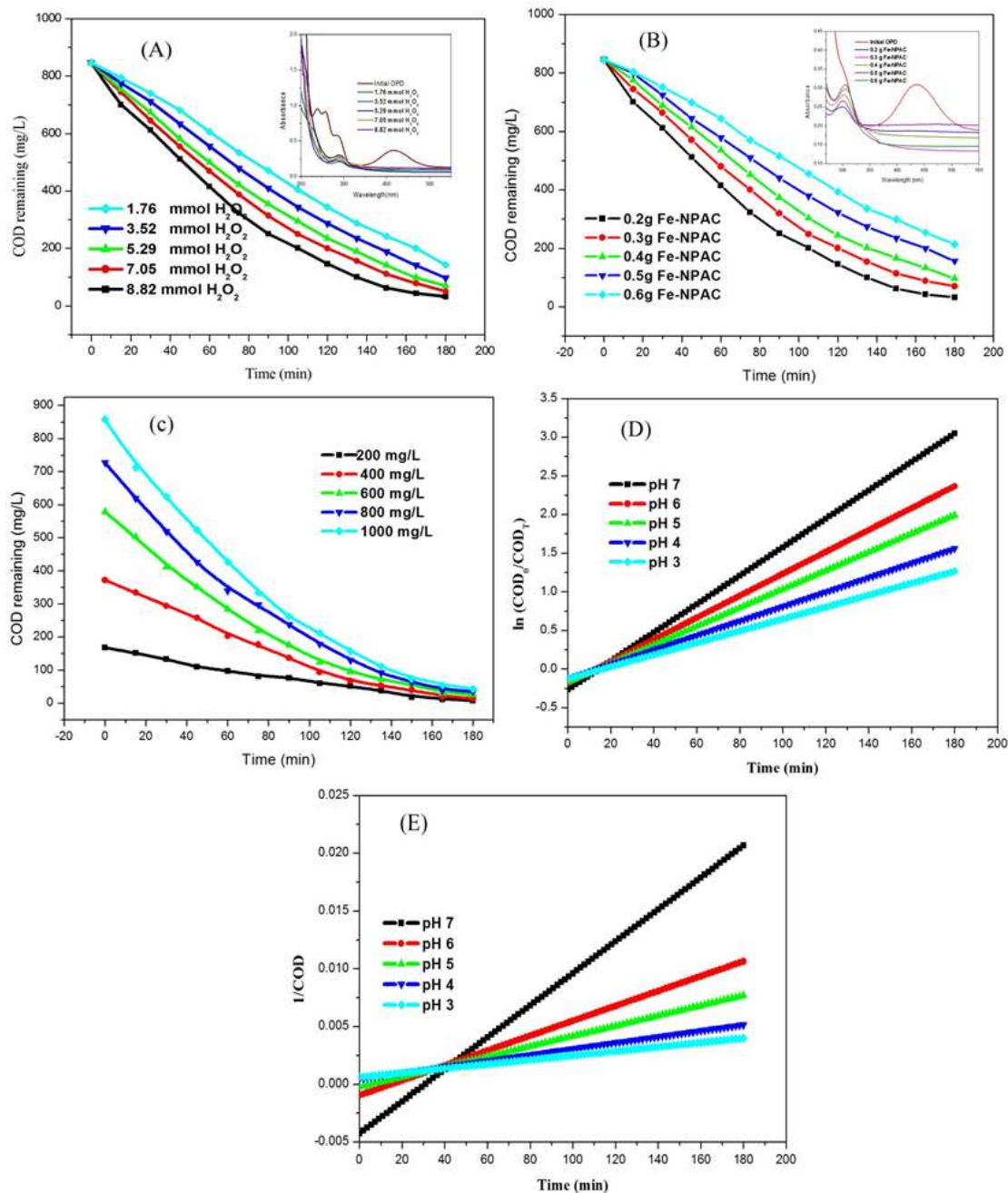


Fig. 6(A) Effect of the concentration of  $H_2O_2$  on OPD efficiency (experimental conditions: Fe-NPAC<sub>400</sub>=0.2g/100ml, OPD =1g/L, pH of suspension = 7 (natural pH)), (B) effect of catalyst (Fe-NPAC) dose on degradation of OPD (experimental conditions:  $H_2O_2$ = 1.764 mmol, OPD =1g/L, pH of suspension = 7 (natural pH)), (C) Effects of different concentrations of OPD (200-1000 ppm) on degradation by Heterogeneous Fenton catalyst Fe-NPAC (experimental conditions: NPAC<sub>400</sub>=0.2g/100ml,  $H_2O_2$ = 1.764 mmol, pH of suspension = 7 (natural pH)), (D,E) First order and Second order kinetics of degradation of OPD over pH with respect to time (min).

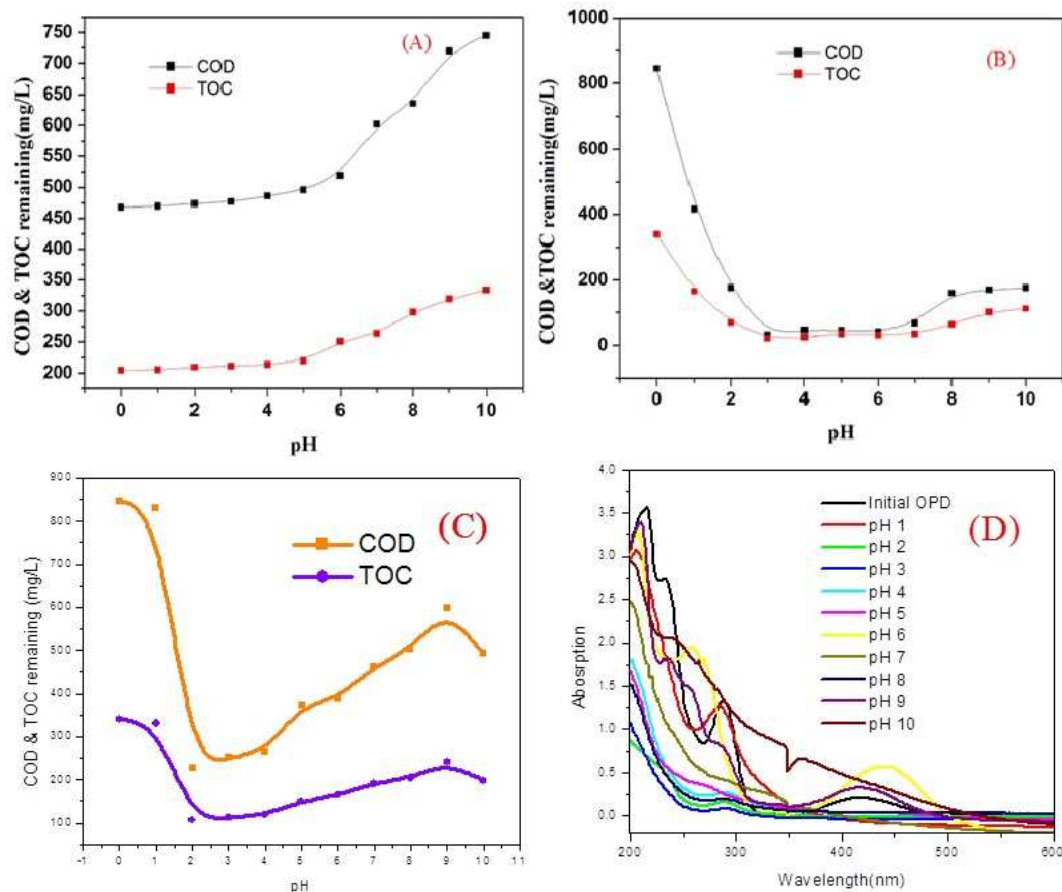


Fig.7 (A) Effect of pH on the degradation of OPD by control Fe-NPAC (OPD+ Fe-NPAC alone), (B) heterogeneous Fenton oxidation (OPD+Fe-NPAC+1.764mmol H<sub>2</sub>O<sub>2</sub>), (C) Homogeneous Fenton oxidation (OPD+FeSO<sub>4</sub> .7H<sub>2</sub>O+1.764mmol H<sub>2</sub>O<sub>2</sub>) under room temperature and the plot showed the COD & TOC remaining versus pH, (D) UV-Visible spectrum of heterogeneous Fenton oxidation (OPD+Fe-NPAC+1.764mmol H<sub>2</sub>O<sub>2</sub>)

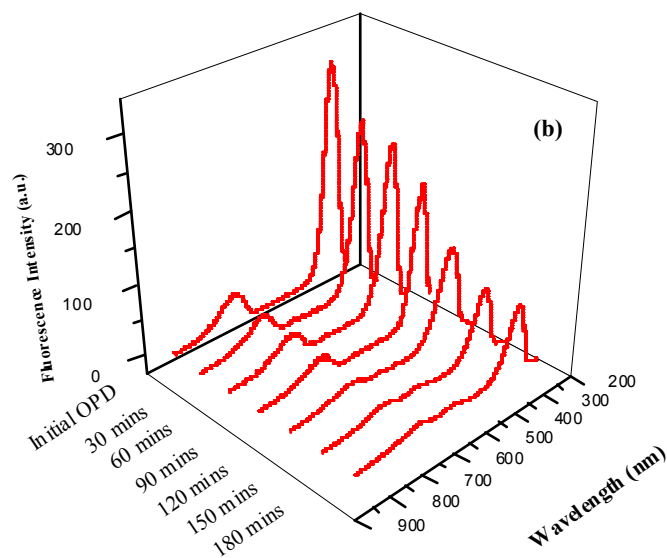
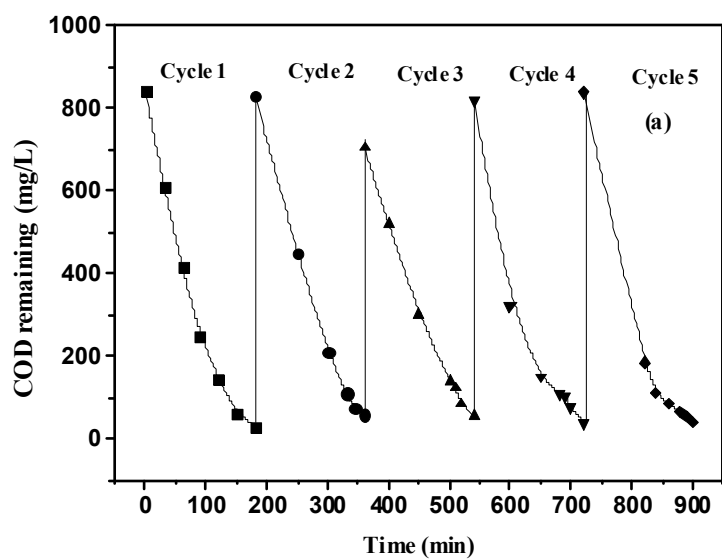


Fig.8a Reusability of Fe-NPAC<sub>400</sub>, Fig.8b Three-dimensional emission fluorescence spectroscopy (OPD before and after Fe-NPAC<sub>400</sub> treated water)

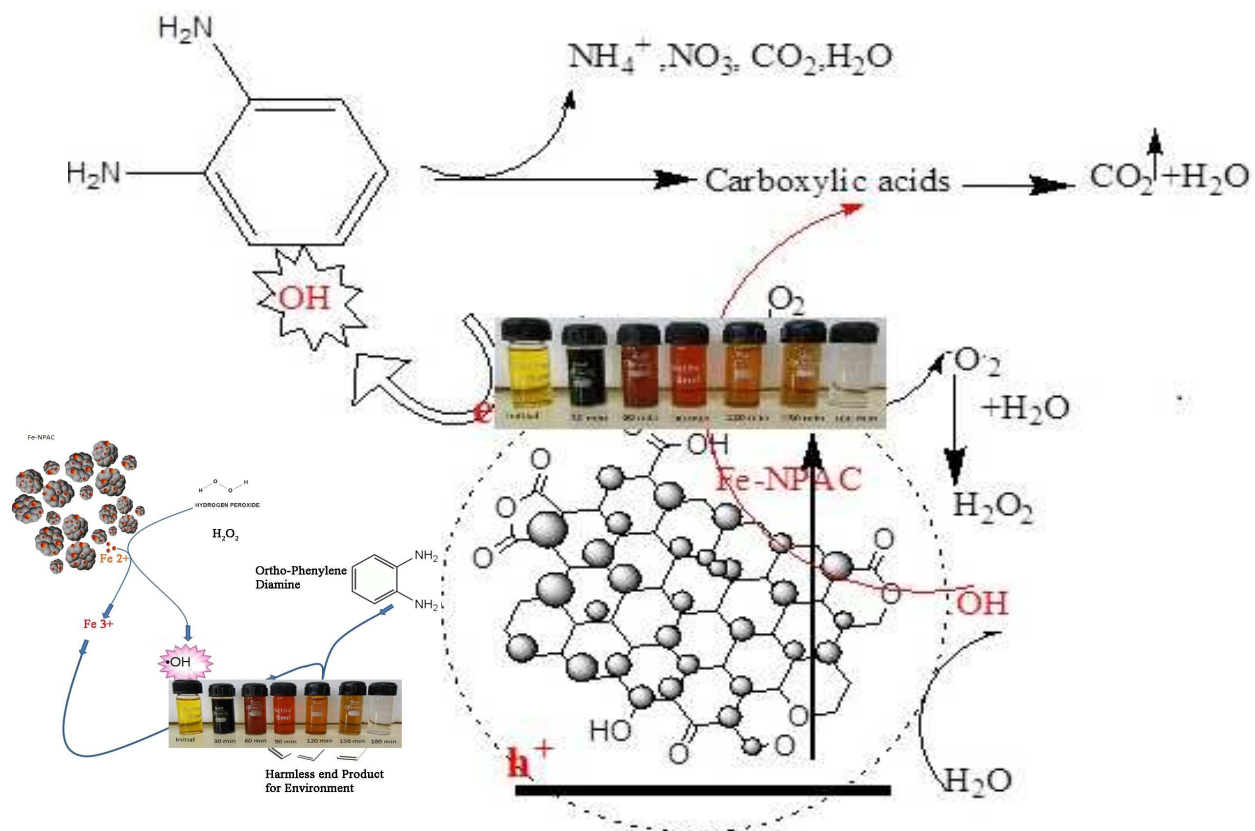
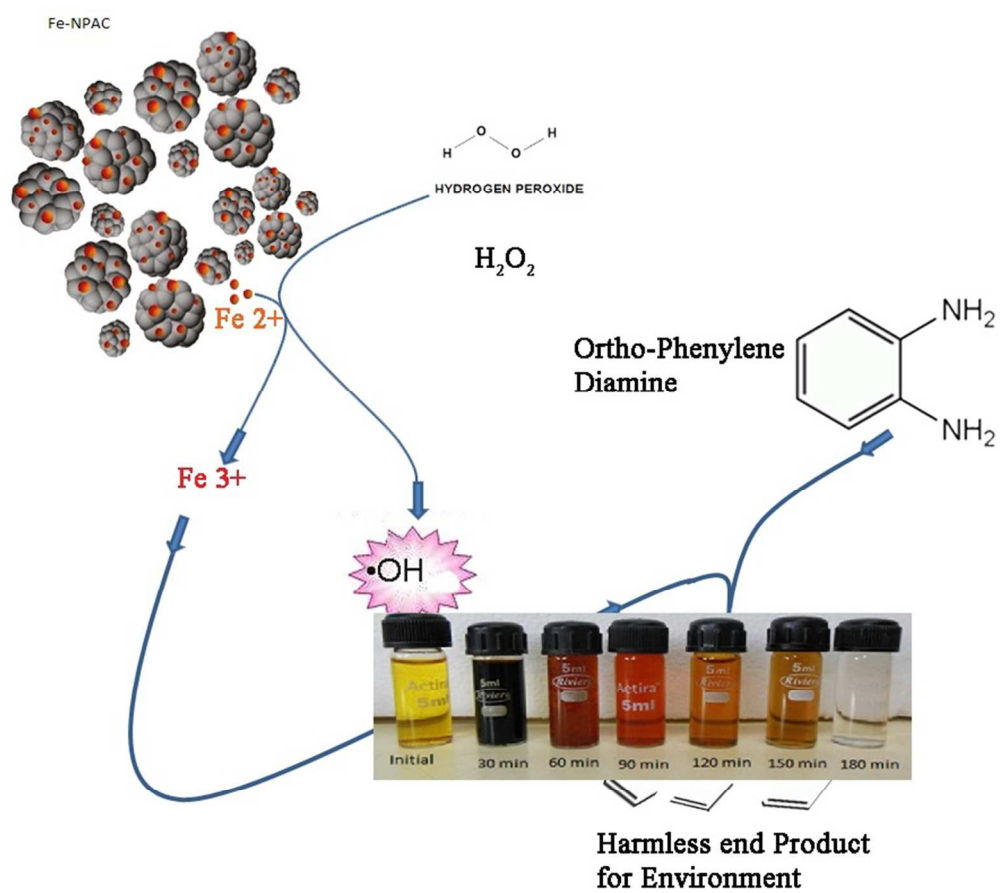


Fig.9 Proposed reaction path way for OPD oxidation by Fe-NPAC catalyst



Proposed reaction path way for OPD oxidation by Fe-NPAC400 catalyst  
74x67mm (300 x 300 DPI)